New Journal of Physics
The open-access journal for physics

Evolution of electronic structure in $Ca_{2-x}Sr_xRuO_4$ observed by photoemission

Shancai Wang and Hong Ding
Department of Physics, Boston College, Chestnut Hill, MA 02467, USA
E-mail: dingh@bc.edu

New Journal of Physics **7** (2005) 112
Received 2 February 2005
Published 29 April 2005
Online at http://www.njp.org/
doi:10.1088/1367-2630/7/1/112

Abstract. We report a systematic angle-resolved photoemission study in $Ca_{2-x}Sr_xRuO_4$ for a wide range of Sr concentrations ($0.3 \leqslant x \leqslant 2.0$), with a focus on the Fermi surface (FS) topology at $x = 0.5$, which is believed to be a quantum critical point. While the dispersion of the valence bands formed by the t_{2g} orbitals is observed to be similar for all Sr levels, the low-energy quasi-particle (QP) weight changes significantly with x. At $x_c = 0.5$, all the three t_{2g} bands, γ (d_{xy}), α, β (mixing of d_{yz} and d_{zx}) remain metallic, with no major electron transfer among them. This is in contrast to the scenario of orbital-selective Mott transition proposed to explain the critical behaviour at $x_c = 0.5$. There is a mild change on the γ FS, which changes to hole-like in $Ca_{1.5}Sr_{0.5}RuO_4$ from electron-like in Sr_2RuO_4. The doping dependence of the QP weight has a general trend of decreasing with decreasing x, but there is a local maximum at $x = 0.5$. This suggests that the QP weight is controlled by the competition between Mott localization and disorder-driven localization.

PII: S1367-2630(05)94145-1

Contents

1. Introduction

The appearance of a wide range of ground states in the 4d transition metal oxide of ruthenate has recently attracted much research attention. By controlling the bonding state in RuO_2 layers and interlayer spacing, the ruthenate system exhibits various kinds of ground states, such as spin-triplet superconductivity, metal with itinerant ferromagnetism, antiferromagnetism and Mott insulating states. Among them, the quasi-two-dimensional system $Ca_{2-x}Sr_xRuO_4$ is a new type of material that connects the p-wave superconductor, Sr_2RuO_4, to the Mott insulator Ca_2RuO_4. The system exhibits many ground states at different Ca concentrations. A systematic study of the electronic structure of $Ca_{2-x}Sr_xRuO_4$ can help understand the metal–insulator transition in strongly correlated systems.

The superconductivity of Sr_2RuO_4 was discovered in 1994 [1]. It is the only non-cuprate perovskite superconductor that is isostructural to the high-T_c cuprate $La_{2-x}Sr_xCuO_4$ and it is thus a good material to compare to high-T_c cuprates. It has a much lower T_c ($\sim$ 1.5 K) than the high-T_c cuprates. However, it is an unconventional superconductor which cannot be explained by BCS theory. The NMR Knight-shift measurement shows no change across T_c, suggesting a non-singlet pairing in the superconducting state [2, 3]. It is believed to be a p-wave superconductor with spin-triplet pairing, possibly mediated by ferromagnetic fluctuations.

The Ca^{2+} ion has the same valence as Sr^{2+}. The substitution of Sr^{2+} by the smaller Ca^{2+} ions does not lead to a more metallic state but to more insulating phases [4, 5]. The phase diagram of $Ca_{2-x}Sr_xRuO_4$ is divided into three regions by its electronic and magnetic properties [6]. They are labelled as region I ($0 < x < 0.3$), region II ($0.3 < x < 0.5$) and region III ($0.5 < x < 2.0$). In region III, the system is basically a paramagnetic metal. The superconductivity is quickly suppressed by a small amount of Ca [5]. At $x = 1.9$, the system is a non-magnetic metal with no superconducting transition. The suppression of superconductivity is believed to be a natural consequence of disorder in a p-wave superconductor. The magnetic susceptibility increases progressively with Ca substitution. It changes from Pauli susceptibility (non-magnetic) to Curie–Weiss form when $x \to 0.5$. The specific heat at low temperature also gets enhanced. In region II ($0.3 < x < 0.5$), the system changes from a non-magnetic metal to a magnetic metal. In region I, a further increase of Ca concentration ($x < 0.2$) changes the system to an antiferromagnetic (AF) insulator at low temperature.

Neutron scattering experiments show that the magnetic properties also change upon Ca substitution [7]. The in-plane susceptibility $\chi(0)$ increases from $x = 2.0$ and reaches its maximum at $x = 0.5$. The Bohr coefficient has a value that corresponds to a local spin moment $S = 1/2$. In region II, the system changes from a non-magnetic metal at high temperature to a magnetic metal across the transition temperature T_o. The transition temperature approaches zero ($T_o \to 0$) when $x \to 0.5$. This is believed to be a quantum transition from a non-magnetic metal to a magnetic metal at $x_c = 0.5$.

Besides the complex phases, there are also structure changes of the system [8]. Sr_2RuO_4 has a K_2NiF_4 structure. With the substitution of Sr by Ca, the RuO_6 octahedra in bulk start to rotate along the c-axis when $x < 1.5$. When $x < 0.5$, RuO_6 starts to tilt from the c-axis in addition to the rotation. When $x < 0.2$, there is additional distortion to the basal plane of the octahedra. Finally at $x = 0$, there is flattening of the octahedra. The Ca substitution also induces disorder in the bulk, whose effect can be reflected from the resistivity measurement. The in-plane residual resistivity can be fitted by Nordheim law $\rho_{ab}(0) = Ax(x - 2)$, indicating a strong disorder effect [5].

The valence band of the ruthenate originates from Ru^{4+} 4d electrons. In Sr_2RuO_4, four 4d electrons are evenly distributed among the three t_{2g} orbitals, d_{xy}, d_{yz}, and d_{zx}, leaving 4/3 electrons in each orbital. The two 1D-like orbitals, d_{yz} and d_{zx}, hybridize and form the α and β bands, while the 2D-like d_{xy} orbital forms the γ band. The electron occupancy is denoted as ($n_{\alpha,\beta}$, n_γ) = (8/3, 4/3) in Sr_2RuO_4.

In Ca_2RuO_4, the reduction of the c-axis length changes the sign of the crystal-field splitting between d_{xy} and $d_{yz,zx}$, so that the d_{xy} orbital is moved to a lower energy than the $d_{yz,zx}$ orbitals. The occupancy is then changed to (2, 2). The bandwidths are also narrower in Ca_2RuO_4 due to the rotation and tilt of RuO_6 octahedra. This effectively increases Hubbard U. The increase of the effective U has two effects: the transfer of electrons among different orbitals and Mott localization of a band when U is larger than its bandwidth. In the case of Ca_2RuO_4, the half-filled $d_{yz,zx}$ orbitals, being Mott localized, along with the completely filled d_{xy} orbital, contribute to the insulating nature of the system.

However, it is not clear how the electronic structure evolves between the two end members. In particular, the knowledge of the electronic structure at $x_c = 0.5$ is crucial in understanding the critical behaviours in $Ca_{1.5}Sr_{0.5}RuO_4$. One theoretical conjecture proposed by Animosov *et al* [9], based on a non-crossing approximation (NCA) calculation within the dynamical mean field theory (DMFT), claims that the electron occupancy should be (3, 1) at $x = 0.5$. The one-hole branch of $d_{yz,zx}$ orbitals is then Mott localized, and result in a local moment $S = 1/2$. However, the half-filled d_{xy} electron remains itinerant due to its wider bandwidth. Therefore, one has the coexistence of metallic transport and local spin moment, which is consistent with experiments [4, 5]. Based on this argument, only the γ Fermi surface (FS) survives at $x = 0.5$, with a smaller occupied volume than in Sr_2RuO_4.

The proposal of an apparent orbital-selective Mott transition (OSMT) is of general interest to the multi-band correlated systems such as transition metal oxides and the heavy fermion compounds. However, the (non-)existence of OSMT, particularly in real materials, has been a much debated issue. In general, localized and extended states cannot coexist at the same energy unless quantum tunnelling (mixing) between these states are strictly forbidden by symmetry considerations.

Indeed, a different quantum Monte Carlo (QMC) calculation within DMFT by Liebsch [10, 11], which considers additional inter-band Coulomb energy, predicts a different result. Under the interaction, the narrow band causes the wide band to become more correlated. At

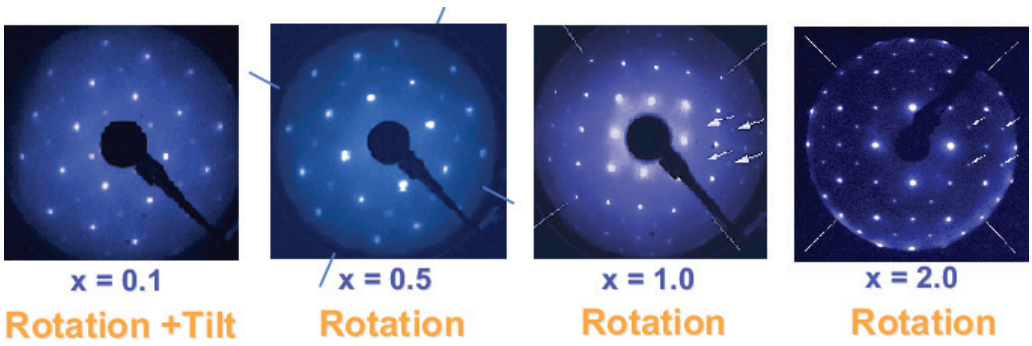

Figure 1. LEED patterns of $Ca_{2-x}Sr_xRuO_4$ at different Sr levels ($x = 0.1, 0.5, 1.0$ and 2.0) show the rotation of RuO_6 octahedra. At $x = 2.0$, the faint dots pointed by arrows indicate the rotation of RuO_6 on the surface. At $x < 1.5$, the faint dots indicate the rotation of RuO_6 which is consistent with the one in bulk.

the same time, the wide band causes the narrow band to become less correlated. This inter-orbital interaction forces one common metal–insulator transition for all sub-bands at the same critical U_c.

The debate on this issue continues with two recent theoretical papers reaching opposite conclusions [12, 13]. However, there has been no experimental test that such OSMT exists in degenerate d-electron systems with a small bandwidth difference among orbitals.

In this paper, we report a systematic angle-resolved photoelectron spectroscopy (ARPES) study on the evolution of the electronic structure of $Ca_{2-x}Sr_xRuO_4$ over a wide Sr concentration ($0.3 \leqslant x \leqslant 2$), with an emphasis on the FS topology at $x_c = 0.5$. The rest of the article is organized as follows: After briefly describing the experimental condition, we present the results in five subsections: (A) check the surface and bulk sensitivity of ARPES results of $Ca_{2-x}Sr_xRuO_4$; (B) evolution of valence bands; (C) low-energy quasi-particle (QP) dispersion; (D) FS topology of $Ca_{1.5}Sr_{0.5}RuO_4$, and its connection to OSMT; (F) evolution of spectral lineshape. In the end, we summarize our main results.

2. Experiments

High quality $Ca_{2-x}Sr_xRuO_4$ single crystals, with $x = 2.0$, 1.9, 1.5, 1.0, 0.5 and 0.3 are prepared by the floating zone method. ARPES experiments are performed at the Synchrotron Radiation Center (University of Wisconsin, Madison, WI). During experiments, several undulator beamlines (NIM and PGM) with different photon energies (10–32 eV) are used. All the samples are cleaved *in situ* and measured at low temperature $T = 20$–40 K in a vacuum better than 8×10^{-11} torr. A Scienta electron analyser capable of multi-angle detection is used with the energy resolution of 10–20 meV and the momentum resolution of ~ 0.02 Å^{-1}.

3. Results

3.1. Surface versus bulk

All $Ca_{2-x}Sr_xRuO_4$ samples studied here are easy to cleave and usually have a flat (0 0 1) surface. The samples exhibit clear LEED patterns for their cleaved surfaces, as shown in figure 1. The

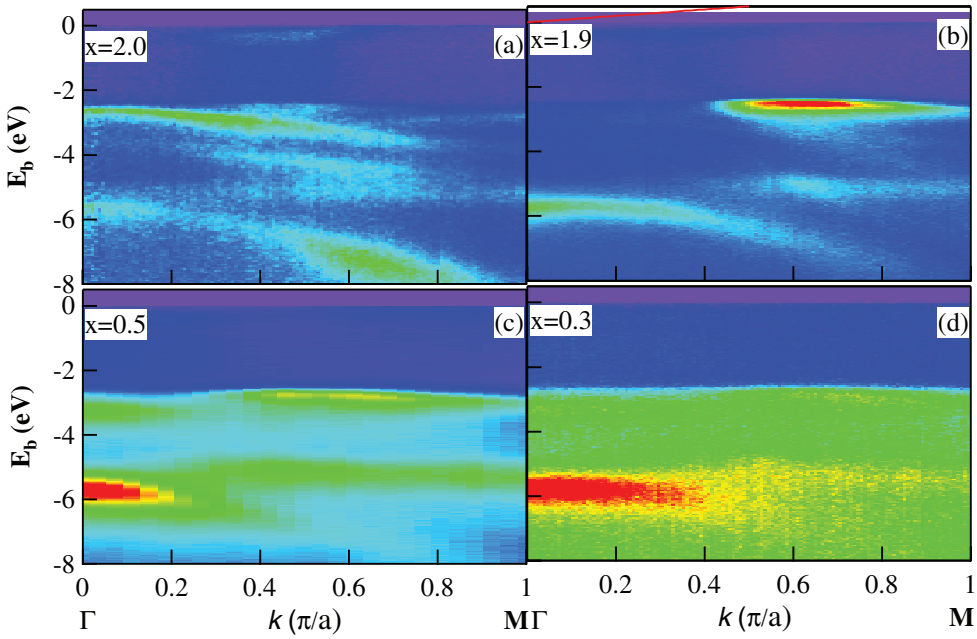

Figure 2. E–k intensity plots of the valence bands of $Ca_{2-x}Sr_xRuO_4$ along Γ–M at (a) $x = 2.0$ ($h\nu = 32$ eV), (b) $x = 1.9$ ($h\nu = 22$ eV), (c) $x = 0.5$ ($h\nu = 32$ eV) and (d) $x = 0.3$ ($h\nu = 21.2$ eV). Note that all intensity colour plots in this paper are linear-scaled false-colour image plots.

brighter LEED spots form a square lattice, corresponding to the 2D RuO_2 lattice. The additional faint spots, which appear in the middle of four bright spots, are caused by the rotation of RuO_6-octahedra along the c-axis. In Sr_2RuO_4, this rotation is caused by a surface reconstruction driven by a soft phonon mode [14]. However, this rotation is observed to exist in the bulk of $Ca_{2-x}Sr_xRuO_4$ when $x < 1.5$ [8].

Due to the rotation of RuO_6-octahedra, the 2D Brillouin zones (BZ) becomes a $\sqrt{2} \times \sqrt{2}$ lattice rotated 45° with respect to the original 1×1 square lattice. Nevertheless, in this paper, we still use the 1×1 square lattice to discuss the band structure for convenience of comparison. The main effect of this rotation on the band structure is a band folding with respect to the new zone boundaries.

As seen from the LEED pattern of $x = 1.0$ sample, the faint points caused by the $\sqrt{2} \times \sqrt{2}$ reconstruction still exist and they are from the bulk. At the critical point $x_c = 0.5$, the rotation angle in the bulk is about 12° [8]. In comparison, the rotation angle on the surface obtained by LEED analysis is about 11°, indicating similar crystal structures between the bulk and the surface. Thus, we expect ARPES results on $Ca_{1.5}Sr_{0.5}RuO_4$ are representative results for the bulk. We have also found that the surface state in Sr_2RuO_4 can be significantly suppressed by either using a certain photon energy (e.g., 32 eV) due to the photoemission matrix element effect, or undergoing a thermal cycle to introduce surface disorder [15].

3.2. Valence-band dispersion

The valence bands of $Ca_{2-x}Sr_xRuO_4$ along the Γ–M (Ru–O bond) direction at different doping levels ($x = 2.0$, 1.9, 0.5 and 0.3) are shown in figures 2 and 3. The valence bands in Sr_2RuO_4

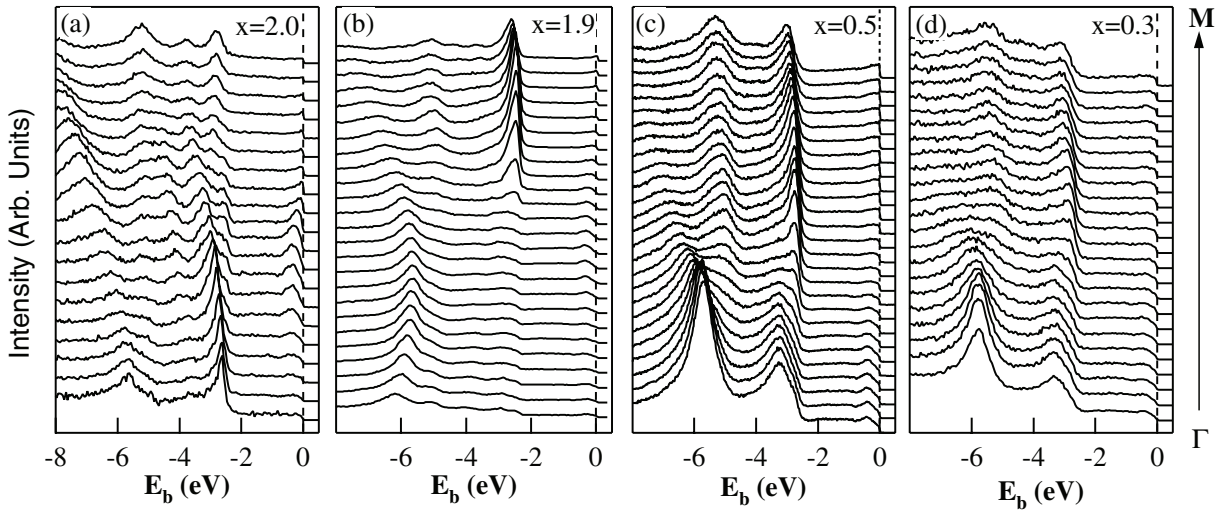

Figure 3. Energy distribution curves (EDCs) of the valence bands of $Ca_{2-x}Sr_xRuO_4$ at different k along Γ–M for (a) $x = 2.0$ ($h\nu = 32$ eV), (b) $x = 1.9$ ($h\nu = 22$ eV), (c) $x = 0.5$ ($h\nu = 32$ eV) and (d) $x = 0.3$ ($h\nu = 21.2$ eV).

can be divided into three regions: the dispersive peaks at high binding energies (6–8 eV), corresponding to the Ru 4dε–O 2pπ bonding orbitals; the weak but dispersive peaks near the Fermi energy (E_F), corresponding to the Ru 4dε–O 2pπ anti-bonding orbitals; the less-dispersive peaks in the middle (2–4 eV), corresponding to the non-bonding O 2p orbitals. For other dopings, the three regions of spectra vary slightly in both energy and intensity. The similar positions and dispersions of the valence bands at different Sr levels indicate no major change of the electron structure by substituting Sr by Ca.

3.3. Low-energy QP dispersion

In the following, we focus on the electronic structure near E_F, which determines the electronic properties of this material. LDA calculations for Sr_2RuO_4 predict two electron-like FSs and one hole-like FS [16, 17]. Quantum oscillation [18] and recent ARPES results [19, 20] agree with the band calculations. The two electron-like FS are the β and γ bands and the hole-like FS is the α band. This is clearly reflected from figure 4(a), where the spectra of Sr_2RuO_4 show two Fermi crossings (β and γ) along the Γ–M direction. The other panels in figure 4 show band dispersion along Γ–M for different Sr contents ($x = 1.9$, 1.5, 1.0, 0.5 and 0.3).

At a high Sr concentration, e.g., $x = 1.9$, the band structure remains essentially the same as in Sr_2RuO_4 but with weaker QP peaks. We find that two bands cross the Fermi level along Γ–M with the same Fermi crossings (k_F) as in Sr_2RuO_4, suggesting that the β and γ bands remain the same. As Sr is further reduced, the band dispersion and the QP peak become less clear. One can only observe the β Fermi crossing along Γ–M at $x = 1.5$ and 0.5. The γ band is absent along this direction. As we will discuss later, our careful ARPES measurements for $x = 0.5$ reveal that the γ FS becomes hole-like, and therefore there is no γ Fermi crossing along Γ–M. For $x = 1.0$ and 0.3, the spectra become so broad that it is difficult to identify band dispersion and FS. This is because of the random disorder introduced by Ca substitution which reaches a maximum at $x = 1.0$, and the Mott localization for $x < 0.5$. More discussions on this will be given below.

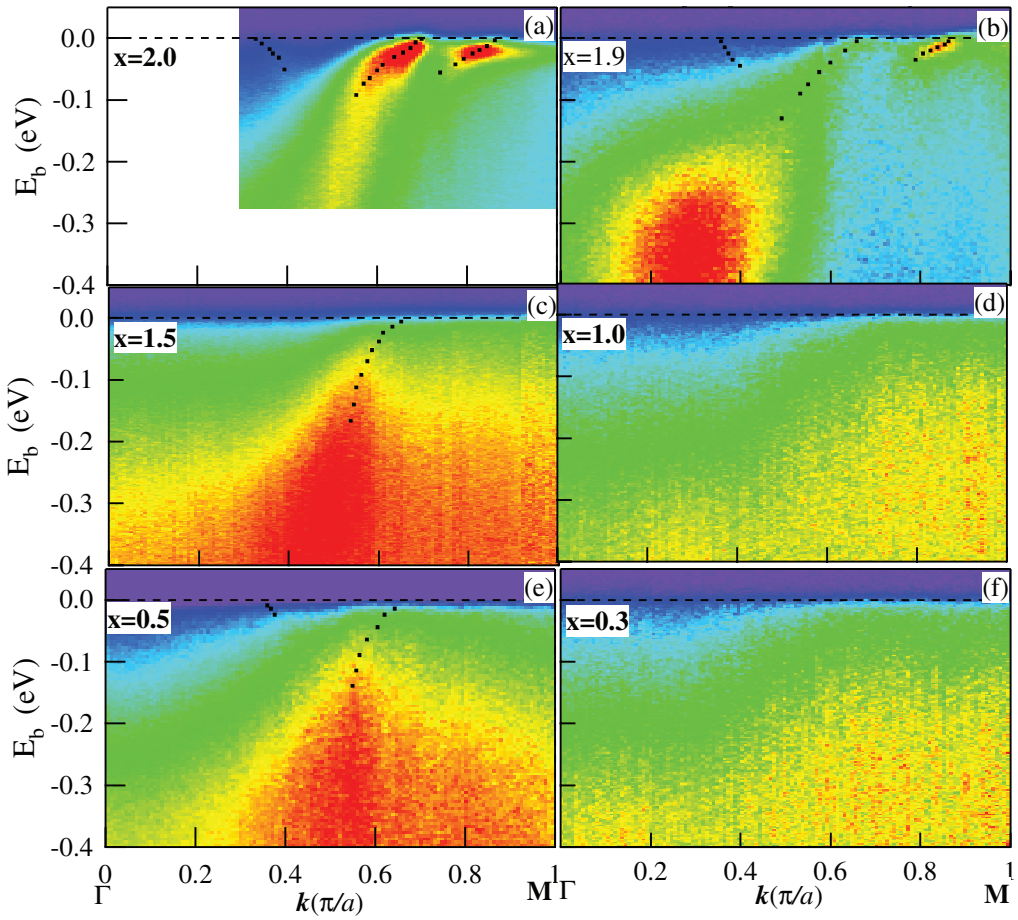

Figure 4. E–k intensity plots near E_F along Γ–M for $Ca_{2-x}Sr_xRuO_4$ at (a) $x = 2.0$ ($h\nu = 32$ eV), (b) $x = 1.9$ ($h\nu = 22$ eV), (c) $x = 1.5$ ($h\nu = 32$ eV), (d) $x = 1.0$ ($h\nu = 21.2$ eV), (e) $x = 0.5$ ($h\nu = 32$ eV) and (f) $x = 0.3$ ($h\nu = 21.2$ eV). The dotted lines are the guides for the band dispersion.

There exists a weak band with a reverse dispersion along Γ–M for $x = 2$, 1.9 and 0.5. In Sr_2RuO_4 and $Ca_{0.1}Sr_{1.9}RuO_4$, it is the reflection of the α band caused by the rotation of RuO_6 octahedra on the surface. For $x = 0.5$, however, this rotation is a bulk property as discussed above. Thus, this α 'image' band is bulk representative.

Figure 5 shows the low-energy band dispersion of $Ca_{2-x}Sr_xRuO_4$ along another high symmetry direction Γ–X. Along this direction, Sr_2RuO_4 has three bands crossing the Fermi level. However, the α and γ bands are very close in k-space. ARPES see only two Fermi crossings along this direction [19, 20], as shown in figure 5(a). The first crossing with $k_F \sim 0.7\pi/a$ is from the β band and the second one with $k_F \sim 1.0\pi/a$ is from both the γ and α bands. Because the d_{xy} orbital has a different symmetry from d_{yz}, d_{zx}, the γ and α FSs can overlap without hybridization. From figures 5(b) and (c), we observe that two similar Fermi crossings of the samples with $x = 1.9$ and 0.5. However, at $x = 0.3$, the spectrum is broad and it is difficult to observe Fermi crossings.

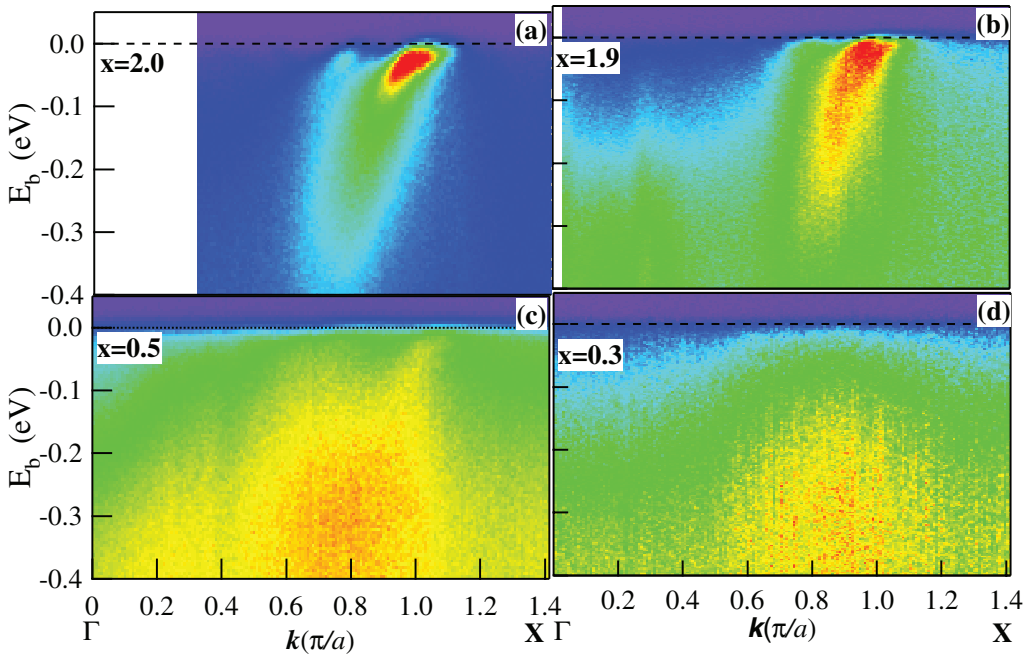

Figure 5. E–k intensity plots near E_F along Γ–Y for $Ca_{2-x}Sr_xRuO_4$ at (a) $x = 2.0$ ($h\nu = 32$ eV), (b) $x = 1.9$ ($h\nu = 21.2$ eV), (c) $x = 0.5$ ($h\nu = 32$ eV) and (d) $x = 0.3$ ($h\nu = 21.2$ eV).

3.4. FS topology in $Ca_{1.5}Sr_{0.5}RuO_4$

The quantum critical point $x_c = 0.5$ is a key point in understanding the evolution of the electronic structure in the ruthenate system and the possible orbital selective Mott transition, as discussed above. We have made careful ARPES measurements on many $Ca_{1.5}Sr_{0.5}RuO_4$ samples. Figure 6 shows the low-energy band dispersion of $Ca_{1.5}Sr_{0.5}RuO_4$ along Γ–M and the comparison to Sr_2RuO_4. In figure 6(a), the EDCs of $Ca_{1.5}Sr_{0.5}RuO_4$ are plotted over several BZs. One can easily observe band dispersion and Fermi crossings. These can be seen more clearly from the 2D E–k intensity plot shown in figure 6(c). From the intensity plot, five bands crossing the Fermi level can be identified, and are marked as #1–#5 respectively. The bands are divided into two types. One type is #1, #3 and #4, and they are from the same band in the reduced zone scheme. Bands #1 and #4 are equivalent to band #3 in different BZs. Based on the band calculation, dHvA measurement, and ARPES results on Sr_2RuO_4, we find that the band identified by #1, #3, and #4 matches the β band. The other type is bands #2 and #5, which have the opposite dispersion. This is the 'image' of the α band caused by the RuO_6 rotation in the material, as discussed above. Note that there should be a similar 'image' band in the first BZ. However, we found that its intensity is too weak to identify due to the matrix element effect in ARPES.

In comparison, an E–k intensity plot of Sr_2RuO_4 along Γ–M is plotted in figure 6(d). In addition to the β band and the 'image' α band, the γ band is also observed near M. However, no such band is visible along Γ–M for $Ca_{1.5}Sr_{0.5}RuO_4$, as shown in figure 6(c).

According to the band calculation, the three FSs are adjacent in the vicinity of $(\frac{2}{3}\pi, \frac{2}{3}\pi)$. Thus, this is a good location to see all the three FSs and their relative positions. This is clearly

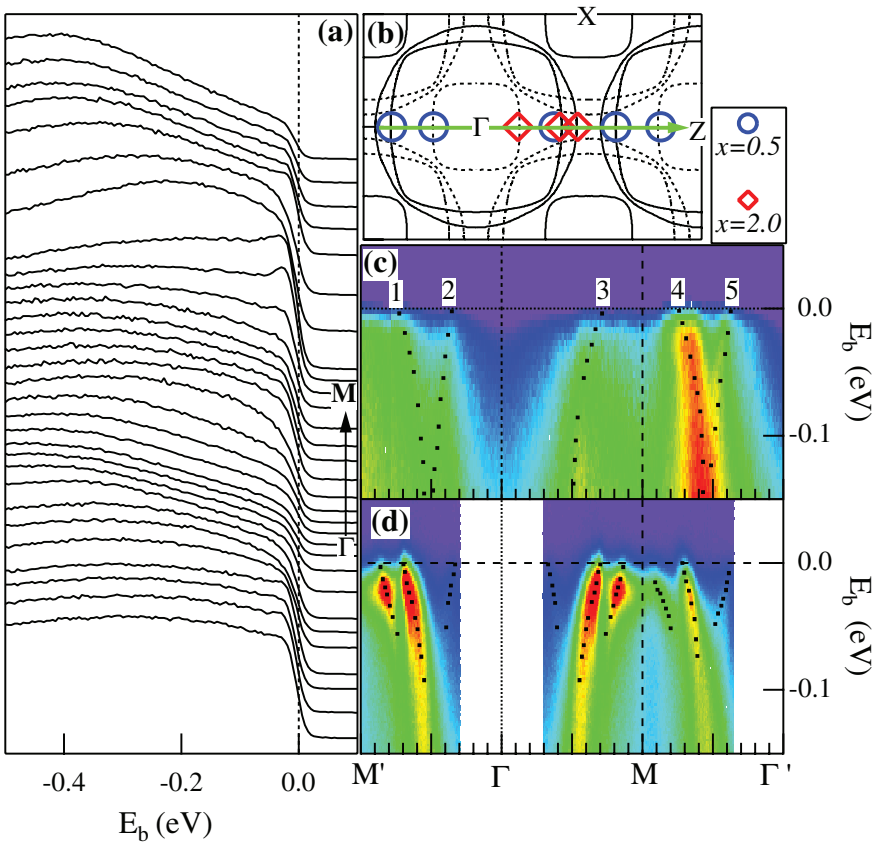

Figure 6. Near-E_F spectra along Γ–M using 32 eV photons. (a) EDCs at different k along Γ–M of $Ca_{1.5}Sr_{0.5}RuO_4$. (b) Measurement locations in extended BZ; with the calculated FSs (——) of Sr_2RuO_4 and the 'image' FSs (- - - -). The FS crossing points extracted from the $Ca_{1.5}Sr_{0.5}RuO_4$ (blue circles) and Sr_2RuO_4 (red diamonds) are shown in extended zone. E–k intensity plots for (c) $Ca_{1.5}Sr_{0.5}RuO_4$ and (d) Sr_2RuO_4.

demonstrated in the case of Sr_2RuO_4, as shown in figure 7(a), where the near-E_F (±20 meV) integration intensity is plotted in a k-region indicated by the shade region (I) in figure 7(c). One can clearly identify all the three FSs and some of their 'image' FSs. Note that the β band is much weaker than the α and γ bands along Γ–X. This is most likely due to the selection rule of ARPES.

In figure 7(b), a similar intensity plot of $Ca_{1.5}Sr_{0.5}RuO_4$ in region (I) is shown. From the plot, one can still observe all the three FSs with a similar k_F, but with weaker intensity than in Sr_2RuO_4. The α band which is centred around $X(\pi, \pi)$ point is clear, with the 'faint' FS almost touching it, which is naturally attributed to the γ FS. The intersection between the α and γ FSs indicates that the d_{xy} and d_{yz}, d_{zx} orbitals still do not mix in $Ca_{1.5}Sr_{0.5}RuO_4$. Another less visible FS which is further separated from the γ and α sheets is assigned to the β band.

As discussed above, we do not observe the γ FS crossing along Γ–M. It is possible that the γ FS changes its topology from electron-like centred at Γ to hole-like centred at X. To check this, we measured ARPES spectra in the vicinity of M, indicated by the rectangular box (II) in BZ shown in figure 7(c). The result is shown in figure 7(d). From the intensity mapping, one

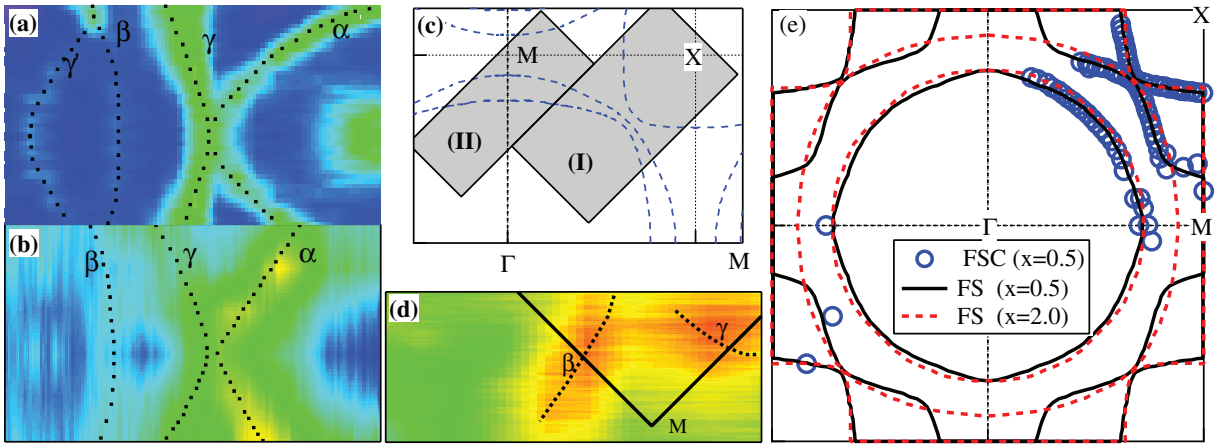

Figure 7. 2D intensity plots integrated over a small energy of E_F (± 20 meV) for (a) Sr_2RuO_4 in the rectangle box (I) indicated in (c); (b) $Ca_{1.5}Sr_{0.5}RuO_4$ in the same box (I); (c) Location of measurement in the BZ; (d) $Ca_{1.5}Sr_{0.5}RuO_4$ in the box (II). (e) Measured FS crossing points (blue circles) and derived FSs (solid black lines) in $Ca_{1.5}Sr_{0.5}RuO_4$. For comparison, extracted FSs (red dashed lines) in Sr_2RuO_4 are also plotted.

can identify that the γ band turns from electron-like in Sr_2RuO_4 to hole-like in $Ca_{1.5}Sr_{0.5}RuO_4$. This is consistent with an LDA calculation based on the rotation of RuO_6 octahedra [21, 22]. In this calculation, the γ band narrows and its van Hove singularity moves below E_F when RuO_6 rotates along the c-axis, which turns the γ FS into hole-like.

The FSs extracted from our ARPES measurements are shown in figure 7(f). The blue open circles are the FS crossing points extracted from figures 6 and 7. The black lines are the reconstructed FSs of $Ca_{1.5}Sr_{0.5}RuO_4$ by smoothly connecting the blue open circles. The FSs of $Ca_{1.5}Sr_{0.5}RuO_4$ can be described as one electron-like (β) and two hole-like (α and γ). The dashed red lines are experimental FSs for Sr_2RuO_4. From the figure, the difference between $Ca_{1.5}Sr_{0.5}RuO_4$ and Sr_2RuO_4 is small except that the γ FS changes from electron-like to hole-like.

From the Fermi topology in figure 7, we extract the values of Fermi vector (k_F) along high symmetry lines and compare them to Sr_2RuO_4. The result is shown in table 1. From the extracted value, we calculated the FS volume enclosed by different bands, and found no significant electron transfer among the three bands. This contradicts the scenario of OSMT. The total occupied area of the two materials is close to 2, which indicates four electrons per unit cell, satisfying Luttinger theorem.

3.5. Evolution of spectral lineshape

In addition to the evolution of band dispersion and FS topology, the spectral lineshape of $Ca_{2-x}Sr_xRuO_4$ changes when x varies, as can be seen in figure 8. We display EDCs on the β FS along Γ–M and Γ–X in figures 8(a) and (b), respectively. While there is a general trend of reduction in the coherent QP spectral weight as x decreases, the QP weight has a local maximum at $x = 0.5$. One likely scenario for this local maximum is due to a competition between disorder-driven and Mott-driven localization. Ca substitution induces random disorder in the bulk, which reaches a maximum at $x = 1$ as indicated by the residual in-plane resistivity [5]. Since

Table 1. k_F of FS crossing points along high symmetry lines, and the occupied FS area in $Ca_{1.5}Sr_{0.5}RuO_4$ and Sr_2RuO_4. The unit of k_F is π/a with $a = 3.76$ (3.86) Å for $Ca_{1.5}Sr_{0.5}RuO_4$ (Sr_2RuO_4).

	$Ca_{1.5}Sr_{0.5}RuO_4$	Sr_2RuO_4
$k_F(x)$ (Γ–M)	$\beta(0.72)$	$\beta(0.72)$, $\gamma(0.88)$
$k_F(x = y)$ (Γ–X)	$\alpha/\gamma(0.67)$, $\beta(0.50)$	$\alpha/\gamma(0.67)$, $\beta(0.51)$
$k_F(y)$ (M–X)	$\alpha(0.62)$, $\gamma(0.22)$	$\alpha(0.64)$
FS area	$\alpha(0.86)$, $\beta(0.38)$, $\gamma(0.68)$	$\alpha(0.86)$, $\beta(0.41)$, $\gamma(0.64)$
Total area	1.92	1.91

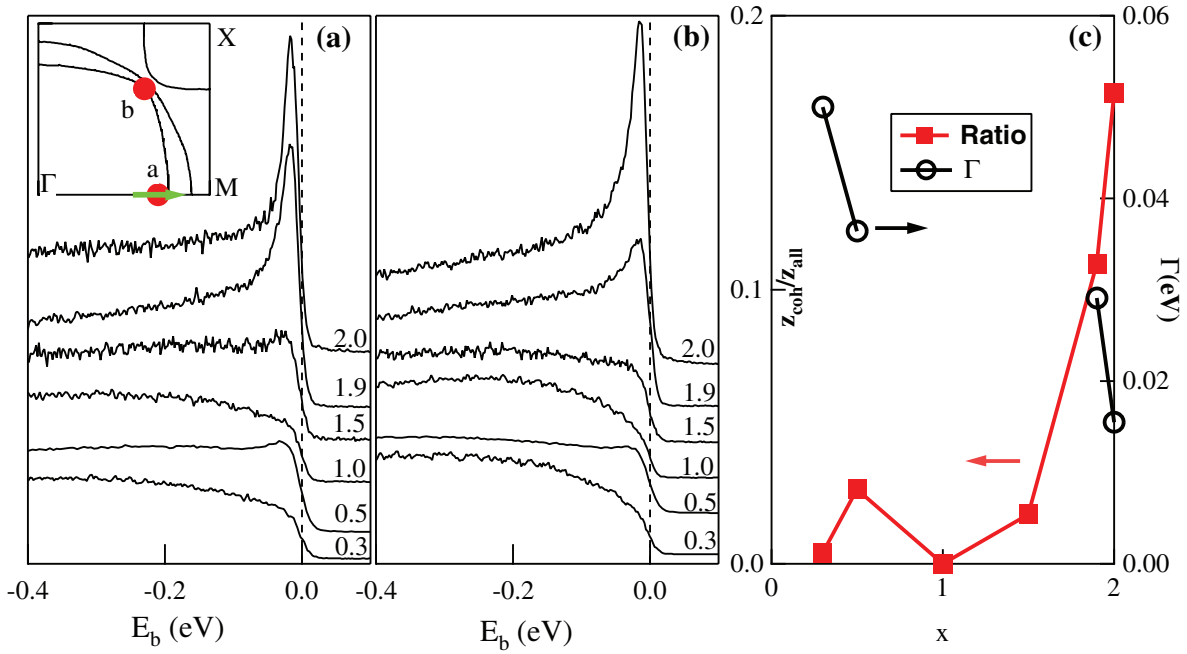

Figure 8. EDCs of $Ca_{2-x}Sr_xRuO_4$ ($x = 2.0$, 1.9, 1.5, 1.0, 0.5 and 0.3) at (a) $k_F(\beta)$ along Γ–M and (b) $k_F(\beta)$ along Γ–X. The measuring points are shown in the inset of (a) and the solid lines in the inset are the calculated FS of Sr_2RuO_4. The phonon energies are 32 eV for $x = 2.0$ and 0.5, and 22 eV for the other Sr levels. (c) Fitting results of QP residue (z) (red squares) and linewidth (Γ) (black circles).

random disorder usually reduces the coherence of QP, this mechanism can naturally explain the observation of the largest reduction of QP weight at $x = 1$, and the symmetrical lineshape between $x = 1.5$ and 0.5. However, the further loss of QP coherence at $x = 0.3$ cannot be attributed to the disorder scattering, instead it is likely caused by Mott localization when AF fluctuations increase in the region of $0.5 > x > 0.2$ and the system becomes an AF Mott insulator for $x < 0.2$.

A fitting procedure is used to extract the doping dependence of the QP lineshape. A spectrum is fitted with a broad incoherent background and a sharp Lorentzian peak, and then modified by the Fermi function. The fitting result along the Γ–X direction is shown is figure 8(c). The data

along Γ–M yield basically the same result. As shown in figure 8(c), the fitting gives a general trend of decreasing QP weight when changing from $x = 2$ to 0.3, but has a local maximum at $x = 0.5$. The QP width (the inverse lifetime) is also plotted in figure 8(c). At doping levels $x = 1.0$ and 1.5, the QP weight is so small that the QP linewidth cannot be reliably extracted.

4. Conclusions

In this paper, we present ARPES results on the evolution of the electronic structure of $Ca_{2-x}Sr_xRuO_4$ ($0.3 \leqslant x \leqslant 2.0$). From our ARPES experiments, there is no major change of the valence bands upon Ca substitution. Compared to $x = 2$, the electronic structure at $x_c = 0.5$ near E_F still has three itinerant bands (α, β and γ). Therefore, our results suggest that there is no orbital selective Mott transition at $x_c = 0.5$. The noticeable change is that the 2D γ FS changes from electron-like to hole-like at $x_c = 0.5$, while the quasi-1D α and β FSs remain essentially the same. There is no significant change of FS volumes for the three bands for $0.5 \leqslant x \leqslant 2.0$, indicating no major electron transfer among the three t_{2g} bands. The QP weight has a general trend of decreasing with Ca substitution, but has a local maximum at $x_c = 0.5$. We propose that this is controlled by the competition between Mott-localization and disorder-driven localization.

Acknowledgments

We thank H-B Yang, A K P Sekeharan, S Souma, H Matsui, T Sato, T Takahashi, C-X Lu, J-D Zhang for experimental collaborations, Z Fang, A Liebsch, A Millis, E W Plummer, T M Rice and Z Wang for discussions and suggestions and R Jin and D Mandrus for providing single crystal samples. This work is supported by NSF DMR-0072205 and DMR-0353108. This work is based upon research conducted at the Synchrotron Radiation Center supported by NSF DMR-0084402.

References

[1] Maeno Y, Hashimoto H, Yoshida K, Nishizaki S, Fujita T, Bednorz J G and Lichtenberg F 1994 *Nature* **372** 532
[2] Ishida K, Mukuda H, Kitaoka Y, Asayama K, Mao Z Q, Mori Y and Maeno Y 1998 *Nature* **396** 658
[3] Ishida K, Mukuda H, Kitaoka Y, Mao Z Q, Fukazawa H and Maeno Y 2001 *Phys. Rev.* B **63** 060507
[4] Nakstsuji S and Maeno Y 2000 *Phys. Rev. Lett.* **84** 2666
[5] Nakstsuji S and Maeno Y 2000 *Phys. Rev.* B **62** 6458
[6] Maeno Y, Nakatsuji S and Ikeda S 1999 *Mater. Sci. Eng.* B **63** 70
[7] Gukasov A, Braden M, Papoular R J, Nakatsuji S and Maeno Y 2002 *Phys. Rev. Lett.* **89** 226401
[8] Friedt O, Braden M, Andre G, Adelmann P, Nakatsuji S and Maeno Y 2001 *Phys. Rev.* B **63** 174432
[9] Anisimov V I, Nekrasov L A, Knodakov D E, Rice T M and Sigrist M 2002 *Eur. Phys. J.* B **25** 191
[10] Liebsch A 2003 *Europhys. Lett.* **63** 97
[11] Liebsch A 2003 *Phys. Rev. Lett.* **91** 226401
[12] Koga A, Kawakami N, Rice T M and Sigrist M 2004 *Preprint* cond-mat/0401223
[13] Liebsch A 2004 *Preprint* cond-mat/0405410
[14] Matzdorf R, Fang Z, Ismail A, Zhang J D, Kimura T, Tokura Y, Terakura K and Plummer E W 2000 *Science*, **289** 746

[15] Wang S-C *et al.* 2004 *Phys. Rev. Lett.* **92** 137002
[16] Oguchi T 1995 *Phys. Rev.* B **51** 1385
[17] Singh D J 1995 *Phys. Rev.* B **52** 1358
[18] Mackenzie A P, Julian S R, Diver A J, McMullan G J, Ray M P, Lonzarich G G, Maeno Y, Nishizaki S and Fujita T 1996 *Phys. Rev. Lett.* **76** 3786
[19] Damascelli A *et al* 2000 *Phys. Rev. Lett.* **85** 5194
[20] Ding H, Wang S-C, Yang H-B, Takahashi T, Campuzano J C and Maeno Y 2001 *Physica* C **364** 594
[21] Fang Z, Nagaosa N and Terakura K 2004 *Phys. Rev.* B **69** 045116
[22] Jung J H, Fang Z, He J P, Kaneko Y, Okimoto Y and Tokura Y 2003 *Phys. Rev. Lett.* **91** 056403